Investigating the Potential of the Low-Cost SDR *USRP B200mini* as an EMI Receiver

Christian Spindelberger, *Student Member, IEEE*, and Holger Arthaber, *Senior Member, IEEE*

***Abstract*—In this article, a compliant radiated emission setup based on a low-cost software-defined radio (SDR) and a transverse electromagnetic cell is presented. The SDR *B200mini* from Ettus Research is investigated, which incorporates the popular Analog Devices *AD9364* transceiver chip. The most demanding requirements for receivers are specified in *CISPR* band C/D. Therefore, the focus is put on the respective frequency range 30 MHz–1 GHz. For performance verification, test signals specified in the dedicated norm *CISPR 16-1-1* are utilized. The results show that the *B200mini* is capable to measure broadband impulses using the peak detector at an analysis bandwidth of 20 MHz. However, downconversion spurs hinder accurate measurements at low tuning frequencies. To overcome this, a highly linear upconversion stage is presented, offering sufficient dynamic range for quasi-peak detector measurements, which are the benchmark for professional receivers. Owing to the bandpass-filtered output of the stage, the SDR must fulfill less stringent linearity requirements, and downconversion spurs become a minor issue. Combining the SDR with the upconversion stage allows one to use full-scale resolution of the implemented analog-to-digital converters (ADCs) without driving the SDR's analog front end into saturation. By decreasing the bandwidth of the ADC's antialiasing filters to 1 MHz, it becomes possible to fulfill quasi-peak detector requirements. Supplementary to *CISPR 16-1-1*, the overall system performance is verified by characterizing a test device. It is shown that the results are comparable with accredited electromagnetic compatibility test houses, enabling a reliable estimate of radiated emission spectra.**

***Index Terms*—*CISPR*, electromagnetic compatibility (EMC), electromagnetic interference (EMI), software-defined radio (SDR), transverse electromagnetic (TEM).**

I. Introduction

ELECTROMANGETIC compatibility (EMC) certification is an inevitable obstacle, which must be passed to commercially sell an electronic product. The constantly evolving requirements, expensive rents for measurement halls, or the unknown performance of a new development are only a few critical examples making this topic challenging. Hence, precompliance measurements have gained a lot of interest by the industry to achieve a competitive time schedule for bringing new or updated products to market. Depending on the test site, e.g., a semianechoic chamber (SAC), it takes a lot of space, several instruments, and trained specialists to obtain accurate results in advance. Small companies, especially start-ups, often do not have the resources to stem such high investments. Owing to missing testing opportunities, the EMC certification process can become a setback for entrepreneurs in holding completion and financial goals.

In the past, a lot of research has been made toward low-cost precompliance equipment for emission testing in laboratory conditions. Compliant conducted tests (9 kHz–30 MHz) are typically made with an inexpensive line impedance stabilization network [1], [2], [3]. Regarding radiated measurements (30 MHz–18 GHz), a large variety of methods exist. For instance, the classic biconical dipole is often used up to 1 GHz. Even though these antennas are low cost and come with calibration data, the limited sensitivity and setup-related uncertainties impede accurate measurements. Recently, reverberation chambers of any kind have gained a lot of popularity. They offer a large test volume relative to their overall size and make high frequencies (>1 GHz) accessible. Unfortunately, a large cavity is required to extend the lower usable frequency making them uninteresting for low budget systems starting from 30 MHz [4]. Thus, transverse electromagnetic (TEM) cells have become the workhorse between 30 MHz and 1 GHz as they perform well at low frequencies, and they are compact in size. Do-it-yourself cells for a budget below 500 have been investigated in [5] and [6].

The still expensive part is the electromagnetic interference (EMI) receiver. According to the norm *CISPR 16-1-1*, broadband impulses have to be measured demanding high linearity requirements [7]. Conventional EMI analyzers usually come with a costly preselection filter bank to measure the specified test signals with sufficient accuracy [8]. Nowadays, broadband sampler architectures are widely used, pushing traditional receivers from the market as they perform frequency scans with exceptional speed [9]. Nevertheless, it has been shown in [10] and [11] that conducted emission tests can be tackled successfully using a standard oscilloscope. Radiated emission tests, however, cover frequencies in the Gigahertz range exceeding the bandwidth and dynamic range (DR) of such an instrument. Promising alternatives to make higher frequencies accessible are software-defined radios (SDRs), which are low-budget and versatile configurable receivers, tunable arbitrarily up to a few gigahertz [12]. In [13], the out-of-the-box performance of popular SDRs as an EMI receiver has been investigated in *CISPR*

Manuscript received 3 April 2023; revised 21 June 2023; accepted 15 September 2023. Date of publication 3 October 2023; date of current version 16 April 2024. This work was supported in part by the Interreg EFRE Foundation through Project AMOR ATCZ-203 and in part by TU Wien Bibliothek through its Open Access Funding Program. *(Corresponding author: Christian Spindelberger.)*

The authors are with the Department of Electrodynamics Microwave and Circuit Engineering, Vienna University of Technology, 1040 Vienna, Austria (e-mail: christian.spindelberger@tuwien.ac.at; holger.arthaber@tuwien.ac.at).

Color versions of one or more figures in this article are available at https://doi.org/10.1109/TEMC.2023.3317731.

Digital Object Identifier 10.1109/TEMC.2023.3317731

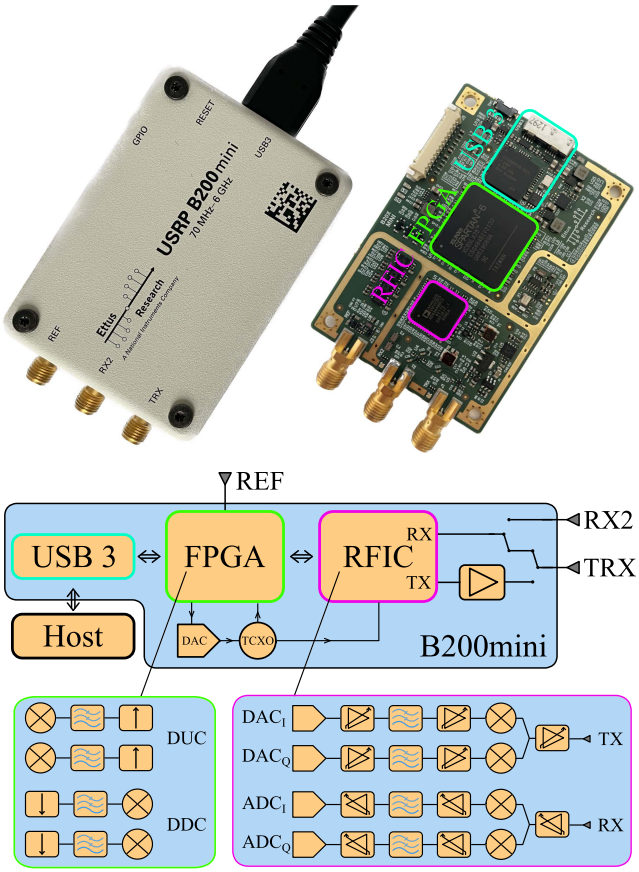

Fig. 1. (Top) Picture of the *B200mini*. (Bottom) Block diagram describing the main functionalities of the SDR.

band C/D (30 MHz–1 GHz). The results indicate that SDRs have the potential to be used for radiated emission testing. As purely homodyne receivers suffered significantly from downconversion spurs and a limited DR, a front-end extension was presented in [14] to improve the performance. The novelty of this work comprises the investigation of a low-cost SDR in conjunction with a redesigned version of the proposed front-end extension to make complaint measurements in *CISPR* band C/D possible.

In our work, the *B200mini* from Ettus Research (see Fig. 1) is analyzed as it is based on the RFIC *AD9364* from Analog Devices, which is used in many other SDRs, e.g., in the *PlutoSDR* or *bladeRF 2.0 micro*. The RFIC provides full-duplex operation and has a purely homodyne receiver and transmitter path. It is possible to tune the gain and bandwidth parameters individually. A field-programmable gate array (FPGA) exchanges the data between the RFIC and the host over the USB 3 link and allows one to perform operations on the sampled data, e.g., decimation, interpolation, digital down, or upconversion. The entry-level price for such an SDR starts from approximately 350€ .

The main target of this work is to elaborate on the limits of the low-cost SDR *B200mini* as an EMI receiver and how the performance can be improved with the introduced hardware extension. The rest of this article is organized as follows. First, the *B200mini* is analyzed alone, according to the most important EMC norms related to TEM cells as test setup, in Section II. In Section III, the second part, a redesigned version of the hardware extension is presented and characterized. Next, the SDR and the extension are analyzed in combination, and the achieved improvements are discussed in Section IV. As a last step in Section V, the overall system performance is verified under realistic conditions by measuring the emission spectrum of an equipment under test (EUT). Finally, Section VI concludes this article.

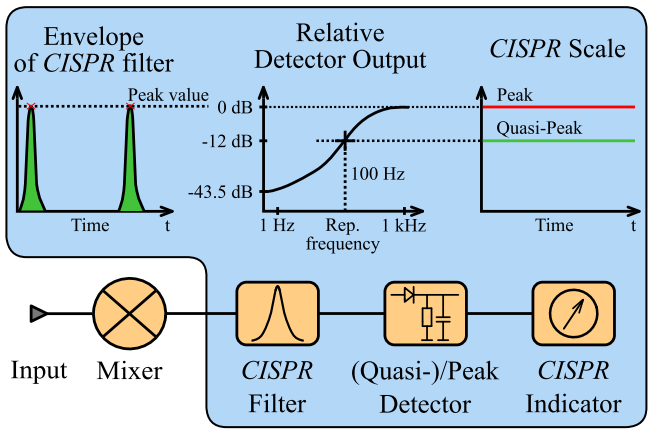

Fig. 2. Block diagram of an EMI receiver.

II. Requirements and Performance

The most important norm EMI receivers have to fulfill is *CISPR 16-1-1*. Based on a black-box approach, the analyzer is exposed to certain test signals to verify compliance. Radiated emission measurements start at 30 MHz and go up to 18 GHz. The most demanding requirements for the EMI receiver's analog front end are defined in *CISPR* band C/D, reaching from 30 MHz to 1 GHz. Owing to a certain detector, called quasi-peak detector (QPD), the front end has to provide superior linearity representing the benchmark for such equipment.

In the addressed frequency range, TEM cells are a very popular test site for precompliance purposes. Presently, they are accepted as a compliant method, e.g., in *CISPR 32*, a radiated emission norm applied for multimedia equipment [15]. In the following, the *B200mini* is analyzed in conjunction with a TEM-cell-based setup in *CISPR* band C/D, configured as the image-reject receiver.

A. CISPR Filter and Detectors

EMI receivers differ from classical swept spectrum analyzers as they stay tuned at a certain frequency f_0 until the signal is detected properly (see Fig. 2). The input signal $x_{\mathrm{RF}}(t)$ is shifted in the frequency domain to the center frequency of the intermediate frequency (IF) filter ($h(t)$, *CISPR* filter), where $\mathcal{H}\{\cdot\}$ denotes the Hilbert transform

$$x_{\mathrm{IF}}(t) = \frac{1}{2}(x_{\mathrm{RF}}(t) + j\mathcal{H}\{x_{\mathrm{RF}}(t)\})e^{-j2\pi(f_0 - f_{\mathrm{IF}})t}$$
$$= \frac{1}{2}x_A(t)e^{-j2\pi f_{\mathrm{LO}}t}. \quad (1)$$

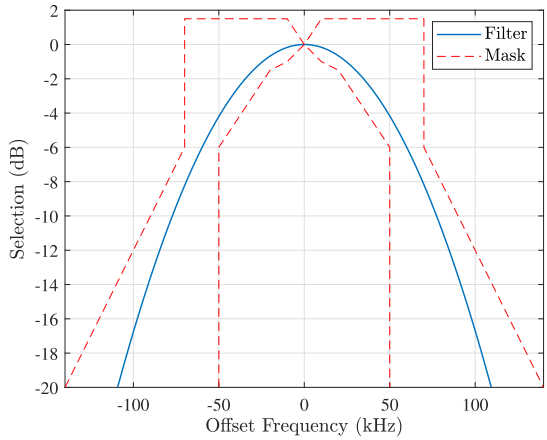

Fig. 3. Selection curve and spectral mask of the 120-kHz filter for *CISPR* band C/D.

After the convolution with $h(t)$, the signal's envelope is processed by the detector $\mathcal{D}\{\cdot\}$, and the result is indicated according to

$$I_{f_0} = \mathcal{D}\{|x_{\mathrm{IF}}(t) * h(t)|\} = \mathcal{D}\{|x_{\mathrm{D}}(t)|\}. \tag{2}$$

The utilized analysis filter has to comply with a spectral mask given in Fig. 3. In digital IF receivers, it is common practice to use a Gaussian transfer curve according to the function

$$h(t) = 2\sqrt[4]{\pi}B_6 \exp\left(-2\sqrt{\pi}(B_6 t)^2\right)$$
$$\circ\!\!-\!\!\bullet \qquad H(f) = \exp\left(-\sqrt{\frac{\pi^3}{4}}\frac{f^2}{B_6^2}\right). \tag{3}$$

In *CISPR* band C/D, the specified 6-dB bandwidth is $B_6 = 120$ kHz. The noise and impulse bandwidths are $B_{\mathrm{N}} = 90.3$ kHz and $B_{\mathrm{I}} = 127.7$ kHz, respectively. In this frequency range, the peak detector (PD) and the QPD are used most frequently. Their response to three different signal types has been analyzed in [16], which are discussed hereinafter for radio frequency (RF)-link budget calculations. As long as the signal envelope is constant, the same power level is indicated by both the detectors. In case of recurrent impulses, the PD holds the maximum of the signal envelope, while the QPD weights the envelope depending on the repetition rate. According to *CISPR 16-1-1*, the QPD may indicate 43.5 dB less than the PD. To prevent preceding receiver elements from saturation, the overload factor (OVF), covering this additional DR, is defined and corresponds to a compression of 1 dB from linear gain. For the PD, an OVF ≥ 0 dB is required as no additional weighting is performed. As the OVF for the PD is the smallest of all the EMI detectors, it has the lowest requirements. Furthermore, it is shown that the QPD amplifies thermal noise by $G_{\mathrm{N}}^{\mathrm{QPD}} = 5$ dB. Regarding the PD, it was demonstrated in [17] that the PD enhances the noise floor by $G_{\mathrm{N}}^{\mathrm{PD}} = 10$ dB compared to the RMS power level.

Throughout this article, it is often referred to the mentioned parameters and functional blocks from Fig. 2 to declare DR definitions. For the interested reader, further details on the implementation of the indication instrument and the QPD are given in [18].

B. Frequency Accuracy

While absolute and relative frequency tolerances are covered in *CISPR 16-1-1*, no considerations on the phase noise are mentioned. Implicitly, the absolute frequency accuracy of the local oscillator (LO) must be precise enough to achieve a maximum tolerance of $\pm 2\%$. In addition, an absolute level accuracy of ± 2 dB has to be achieved by the receiver. The latter requirement can be directly translated into the necessary frequency resolution of the receiver's LO. The selectivity of the *CISPR* filter, defined by (3), allows a maximum frequency step size < 70 kHz to keep the error within the mentioned bound.

In the RFIC *AD9364*, fractional phase-locked loops (PLLs) are used for frequency generation achieving a frequency resolution of 2.4 Hz [19]. Furthermore, the digital down conversion (DDC) allows one to improve the accuracy by shifting the IF. In this article, the *B200mini* is interfaced with the *UHD* framework, supplied by Ettus Research. The driver's frequency tuning routine was used achieving an overall resolution in the millihertz range. Hence, the derived maximum frequency step size is easily achieved.

The *B200mini* incorporates a 40-MHz TCXO as clock reference having a frequency error of $\epsilon_{\mathrm{TCXO}} = \pm 2$ ppm. As the SDR's frequency resolution is more than six magnitudes below the addressed frequency range of *CISPR* band C/D ($\epsilon_{\mathrm{SDR}} < \pm 1$ ppm), the absolute frequency tolerance is kept below the required $\epsilon_{\mathrm{SDR}} + \epsilon_{\mathrm{TCXO}} \leq \pm 2\%$.

C. Continuous Wave Signals

Compliant receivers have to fulfill one main requirement for continuous wave (CW) signals. The suppression of unwanted signal components falling into the IF through, e.g., leakage, image frequencies, or intermodulation, has to be at least 40 dBc.[1] To verify this, the receiver is tuned to a certain frequency f_0 measuring a single tone $x_{\mathrm{RF}}(t) = \cos(2\pi f_0 t)$. Then, the tone is set to different frequency spots of interest $f_{\mathrm{RF}} \neq f_0$ with equal amplitude to measure the relative suppression

$$s = 20\log_{10}\frac{I_{f_0|f_{\mathrm{RF}}=f_0}}{I_{f_0|f_{\mathrm{RF}}\neq f_0}} \leq 40 \text{ dBc}. \tag{4}$$

To compensate frequency-dependent deviations of the setup, the tone's amplitude was calibrated using a power meter.

With the noise gain G_{N}, the minimum required DR in front of the detector can be calculated. For the PD and the QPD, respectively, at least a DR of 50 and 45 dB is necessary. The *B200mini* has a 12-bit continuous sampling delta-sigma analog-to-digital converter (ADC) of third order implemented with a configurable sampling rate. As recommended by Ettus Research, the sampling rate was set to $f_s = 56$ MSa/s. To achieve the required suppression of aliases, the low pass in front of the ADC was set to 22.5 MHz. The lower sideband of the sampled data is investigated achieving a usable analysis bandwidth (ABW) of 20 MHz centered around an IF of $f_{\mathrm{IF}} = -12$ MHz. With the specified filter from (3), the achieved DR of a single tone

[1] The linear signal model from Section II-A describes the detection process and does not take receiver imperfections into account.

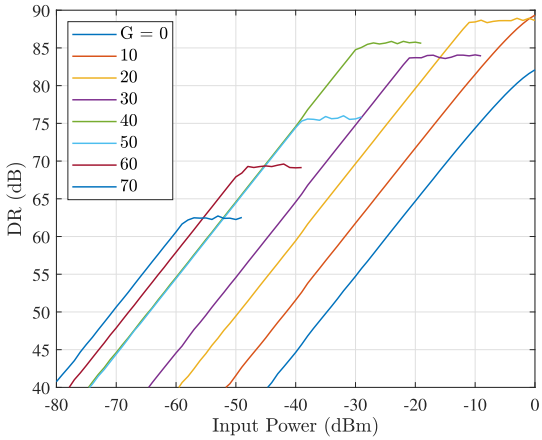

Fig. 4. Measured DR for CW signals over input power for different gain settings.

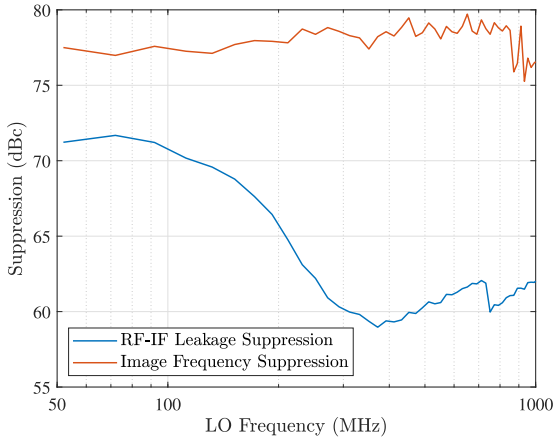

Fig. 5. RF-IF leakage and image frequency suppression over LO frequency.

over input power was measured for different gain settings at $f_0 = 750$ MHz. The results in Fig. 4 show that a sufficient DR is available to verify compliance for CW signals. The power sweep was aborted 10 dB above full-scale reading of the ADC, which is indicated by the compression at the end of the traces. It is to be noted that the gain settings are unitless and only approximately translate into relative gain differences in decibel. The RFIC *AD9364* has three different gain stages, which are mapped to the adjusted settings by an optimized lookup table, supplied by the manufacturer. Gain settings above 50 have a strongly decreasing DR as thermal noise exceeds the quantization noise level. The traces for $G = 40$ and 50 overlap as only the last amplifier in the receiver chain is adjusted, which has no effect on the overall sensitivity. Owing to the higher gain, the full-scale level of the ADC is reached for lower power values.

Assuming that the quantization noise to be uncorrelated and spurious emissions are negligible, it is possible to estimate the effective number of bits (ENOB) of the ADC by using the noise bandwidth B_N of the *CISPR* filter

$$\mathrm{ENOB} = \frac{\mathrm{DR_{CW}} - 1.76\ \mathrm{dB} - 10\log_{10}\left(\frac{f_s}{B_\mathrm{N}}\right)}{6.02\ \mathrm{dB}}. \tag{5}$$

The gain settings between 10 and 20 show the largest DR and give an ENOB of approximately 10 bit.

Owing to the homodyne-based receiver front end of the RFIC *AD9364*, interference through image frequencies has to be expected. The *B200mini* uses an internal calibration routine to compensate I/Q imbalances. To perform a frequency scan over *CISPR* band C/D with the achieved ABW, the LO must be tuned between 52 and 1002 MHz. Over the complete LO tuning range, the suppression of images $I_{f_0|f_\mathrm{RF}=f_0}/I_{f_0|f_\mathrm{RF}=f_0-2f_\mathrm{IF}}$ was verified to be larger than 75 dB. In addition to this, the suppression of RF–IF leakage $I_{f_0|f_\mathrm{RF}=f_0}/I_{f_0|f_\mathrm{RF}=f_\mathrm{IF}}$ was measured and depicted in Fig. 5. As the results are well above the required 40 dBc, this part is considered to be fulfilled.

Downconversion spurs are a severe problem for homodyne receivers. Frequency content located at LO harmonics interferes in baseband with the fundamental conversion product. This behavior further aggravates as LO harmonics are intentionally produced to increase the DR of the mixer using a rectangular signal [20]. The suppression is measured by setting the interfering tone to integer multiples of the LO according to $I_{f_0|f_\mathrm{RF}=nf_\mathrm{LO}\pm f_\mathrm{IF}}$, where the positive sign of the IF stands for the image frequency. The suppression is depicted in Fig. 6. It was found out that especially odd-order modulation products cause the most problems. Furthermore, maximum interference occurs for tones located at multiples of the image frequency for $n = 3$ and 7. Obviously, the *CISPR 16-1-1* norm is not achieved. This problem can be mitigated by preselection filtering to suppress frequency content at LO harmonics. The main downside of this approach is that a large number of filters are required for sufficient suppression even at low tuning frequencies.

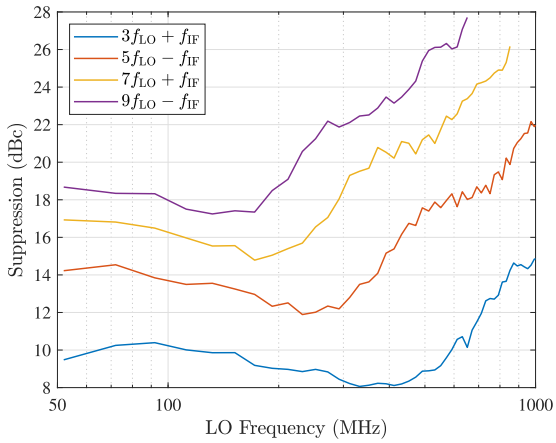

Fig. 6. Suppression of interference according to $nf_\mathrm{LO} \pm f_\mathrm{IF}$.

The frequency response of the SDR's antialiasing filter (AAF) showed a negligible ripple justifying that the performance measurements apply over the entire ABW. For frequencies approaching half the sampling rate, a slightly degraded sensitivity has to be expected due to noise shaping lobes of the implemented delta-sigma ADC.

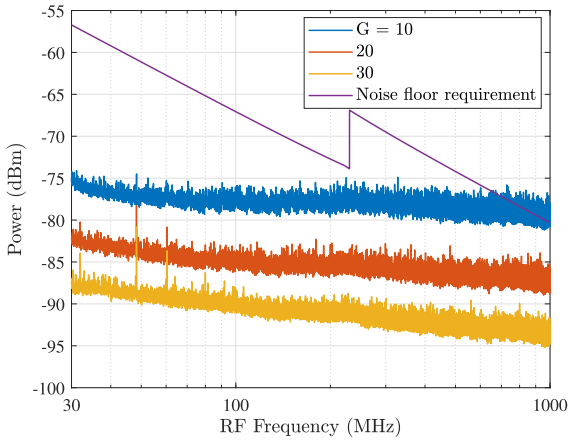

Fig. 7. Peak detected noise floor over *CISPR* band C/D for different gain settings.

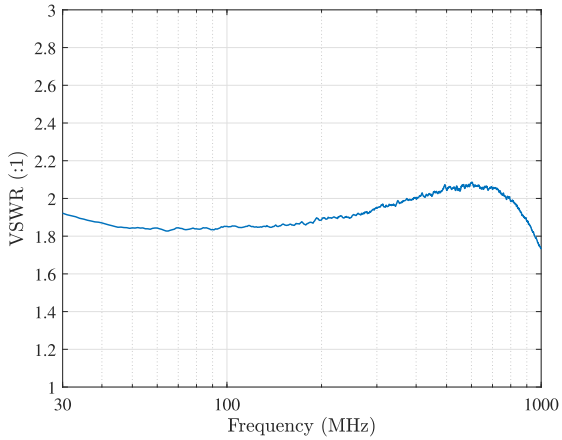

Fig. 8. VSWR of the *B200mini* measured at input RX2.

D. Receiver Sensitivity

Radiated emission limits are usually not explicitly given for TEM cells. As suggested in *CISPR 32*, the results have to be correlated to an SAC with a measurement distance of 10 m. Therefore, the total radiated power of the EUT is recalculated using (6). A detailed description on the derivation of the formula

$$E_{\max} = g_{\max} \frac{60 k_0}{e_{0_y}} \sqrt{\frac{\sum_{i=1}^{3} V_i^2}{Z_0}} \tag{6}$$

can be found in [21]. As long as the EUT may be considered small, the dipole moment is dominant. Measuring three orthogonal positions of the EUT in the TEM cell using one port allows one to estimate the total radiated power $P_{\text{tot}} = \sum_{i=1}^{3} V_i^2 / Z_0$. As the measured voltages V_i are scalar values, it is assumed that the dipole moments are radiating in phase. To relate P_{tot} to field strength values, the factor e_{0_y} is introduced. It can be calculated analytically depending on the cross section of the TEM cell and EUT positioning [22]. For the cell proposed in [6], with a septum height of 300 mm, the field factor in the central is $e_{0_y} = 18\sqrt{\Omega}/\text{m}$. To find the maximum emitted field strength in the SAC, a height scan of the receiver antenna at different polarizations is performed. This procedure is considered with $g_{\max}$. It is assumed that P_{tot} is radiated by a dipole over an infinitely extended ground plane. This scenario is solved analytically with a mirrored dipole. The theoretically maximum received power level for vertical and horizontal polarizations over an antenna height scan between 1 and 4 m yields $E_{\max}$. Further details on the derivation are given in Appendix A.

According to *CISPR 32*, the radiated emission limit for class B devices in an SAC with 10-m distance is 30 dB μ V/m between 30 and 230 MHz and 37 dB μ V/m between 230 and 1000 MHz. Rearranging (6) allows one to calculate $V_{\text{N}} = \sqrt{(V_1^2 + V_2^2 + V_3^2)/3}$, which is the maximum allowed thermal noise voltage not exceeding the defined emission limit. The derived sensitivity limit is compared to the PD noise floor of the *B200mini* for different gain settings in Fig. 7. The signal was analyzed using the short-time Fourier transform with the filter from (3) as windowing function. For the measurement, the SDR was tuned through *CISPR* band C/D making recordings with a length of 1 s. In the frequency domain, a bin resolution of 1 kHz and a bandwidth of 10 MHz were chosen. The overlap of the time sequences was configured to 90%, which is sufficient for a compliant measurement [23].

The lower limit of the EMI receiver indication range is defined by a maximum signal level error of 1 dB. In case of thermal noise, this requires a minimum signal-to-noise ratio (SNR) of 6 dB. If spurious emissions coincide with the signal of interest, an SNR of up to 19 dB may become necessary depending on the signals phases. The results in Fig. 7 indicate that with gain settings between 20 and 30, the sensitivity is high enough to keep the noise floor 6 dB below the calculated sensitivity requirement. The frequency spurs below 100 MHz have their maximum at -78 dBm for gain setting 20, failing the 19-dB rule. Hence, one is best advised to keep the gain at setting 30 for a compliant frequency scan.

E. Voltage Standing Wave Ratio

CISPR 16-1-1 requires a voltage standing wave ratio (VSWR) below 2:1, if no attenuation is inserted at the receiver input. The matching of the *B200mini*, depicted in Fig. 8, did not change for the investigated gain settings 10–30. Out of the box, the matching slightly fails between 400 and 800 MHz. Fortunately, the norm is still fulfilled if the VSWR is smaller than 1.2:1 for an attenuation larger than 10 dB. As this VSWR corresponds to a return loss of approximately 20 dB, it is easily possible to fulfill the norm with a forced match. For gain setting 30 (see Fig. 7), the degraded sensitivity would be still sufficient to perform compliant tests after inserting a 10-dB attenuator.

F. Impulses

EMI often appears in form of transient signals coming from, e.g., switch-mode power supplies or electrical engines. To form a worst case scenario of these sources, *CISPR 16-1-1* specifies a broadband test signal having a flat power spectral density (PSD) up to 1 GHz, which has to be measured with a defined

accuracy α. Neglecting deviations caused by the detector, it is possible to calculate the required DR for impulses at the *CISPR* filter's output using

$$\mathrm{DR} = \mathrm{OVF} + G_\mathrm{N} + \mathrm{SNR}_\mathrm{min}. \tag{7}$$

While the OVF and the noise amplification $\mathrm{G_N}$ have already been determined in Section II-A, the minimum SNR to achieve α has not been introduced yet. In the norm, a total error of $\alpha^\mathrm{PD} = \pm 1.5$ dB regarding the PD is tolerated. Hence, $\mathrm{SNR_{min}}$ has to be at least 4 dB in the presence of thermal noise, resulting in a DR of 14 dB. In case of isolated transients, the QPD indicates 43.5 dB less than the PD. The allowed $\alpha^\mathrm{QPD} = \pm 2$ dB at this operating point requires an $\mathrm{SNR_{min}} = 2.5$ dB and, thus, a DR of 51 dB. As with the derived requirement for the PD it becomes very difficult to detect a receiver overload, an additional margin is introduced targeting a DR of 25 dB.

In the following, the full-scale power level $P_\mathrm{FS} = 4$ dBm of the *B200mini* is used to estimate the available DR of the ADC for the broadband test signal. A detailed description of used simplifications for signal definitions is given in Appendix B. The bandwidth B of the AAFs in front of the ADC and the gain G are two configurable parameters to achieve full-scale resolution. The peak power at the output of a filter relates to $P = 2(v\tau B_\mathrm{I})^2/Z_0$, where $(v\tau)^2/Z_0$ is the PSD of the applied impulse, and B_I is the impulse bandwidth of the investigated filter. In the RFIC *AD9364*, Butterworth filters of third order are implemented [24]. Their impulse bandwidth is linked to traditional 3-dB bandwidth definition by a scalar factor of 1.35. Based on the maximum rated power level of the SDR's front end $P_\mathrm{max} = 0$ dBm and the known impulse bandwidth of the preselection filter $B_\mathrm{I}^\mathrm{PRE}$, it is possible to derive the required gain

$$\mathrm{G} = \mathrm{P_{FS}} - \mathrm{P_{max}} + 20\log_{10}\frac{\mathrm{B_I^{PRE}}}{\mathrm{B_I^{AAF}}}. \tag{8}$$

The noise power is modeled with the linear superposition of the thermal and the quantization noise according to

$$\mathrm{P_N} = 10\log_{10}\left[\left(\frac{\Delta^2}{12Z_0 f_s} + \mathrm{G}\cdot\mathrm{NF}\cdot\frac{kT_0}{2}\right)B_\mathrm{N}^\mathrm{CISPR}\right]. \tag{9}$$

It has been shown in Section II-C that the ENOB is approximately 10 bit, which allows us to calculate the LSB voltage $\Delta = \sqrt{8Z_0\mathrm{P_{FS}}}/2^\mathrm{ENOB}$ used in (9). Now, it is possible to estimate the ADC performance for pulsed signals using

$$\mathrm{DR_{IMP}} = \mathrm{P_{FS}} + 20\log_{10}\left(\frac{B_\mathrm{I}^\mathrm{CISPR}}{2\,B_\mathrm{I}^\mathrm{AAF}}\right) - \mathrm{P_N}. \tag{10}$$

It is assumed that the quantization noise dominates for low gain settings. As the thermal noise power overtakes the quantization noise for high gain values, the available DR decreases. In Fig. 9, the analytically derived DR for impulses is depicted for two different preselection filters and a noise figure (NF) of the analog SDR front end of 10 dB [25]. It is implied that the NF stays constant for every gain setting and that saturation effects are neglected. In advance of verification, it can be seen that the QPD requirements cannot be achieved, unless the preselector impulse bandwidth is reduced to 62 MHz. Furthermore, it is necessary to reduce the AAF bandwidth as well to measure even

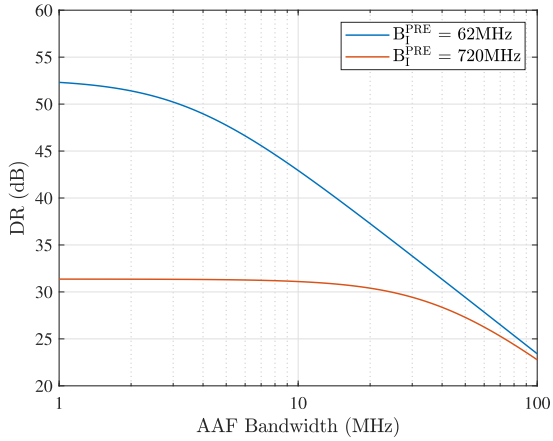

Fig. 9. Analytically derived DR of the *B200mini*'s ADC for different preselector bandwidths.

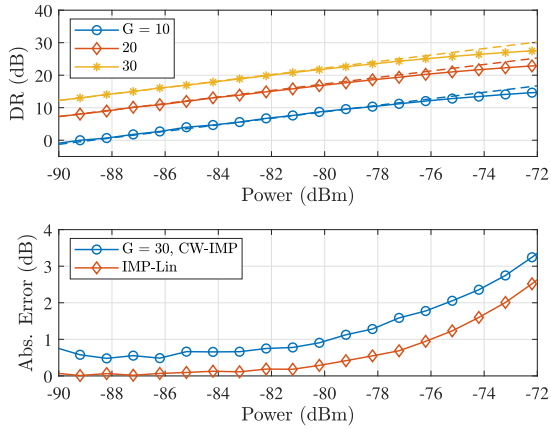

Fig. 10. Broadband DR and compression from linear gain of the *B200mini* over input power.

isolated transients with sufficient accuracy. From the calculations above, it still remains open if the SDR's analog front end can achieve the target DR for broadband impulses using the PD. Therefore, the deviation from linear gain of the peak detected power is measured at $f_0 = 500$ MHz. At the input, a preselection filter covering *CISPR* band C/D and having the assumed $B_\mathrm{I} = 720$ MHz is applied.[2] To reduce power level uncertainties caused by thermal noise, several impulses have been recorded and averaged. In Appendix C, it is explained how the measurement has been performed. The corresponding results are depicted in Fig. 10. It is to be noted that *CISPR 16-1-1* requires to verify the accuracy of the PD by comparing the detected peak power with a calibrated CW signal, ideally indicating the same power level. In the investigated power range, the CW tone is close to the SDR's noise power level. Owing to potential interference buried in noise, deviations in the measured tone envelope have to be expected. Furthermore, higher order conversion products might cause an amplitude error of the detected peak power of the impulses. To emphasize this problem, the deviation from linear gain of the impulses (IMP-Lin) is compared to the absolute error

[2]Bandpass filter: Mini-Circuits, *ZABP-510-S+*, 20 MHz–1 GHz.

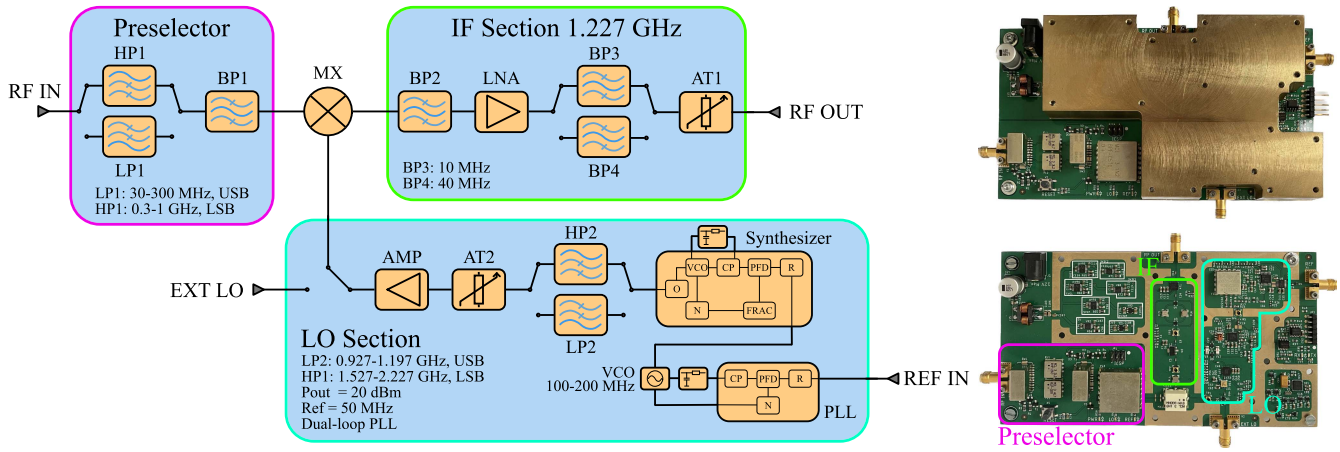

Fig. 11. Block diagram of the implemented upconversion stage (left) and a picture of the realization with and without shielding (right).

taking the calibrated CW signal into account (CW-IMP). While the IMP-Lin trace is monotonically increasing as expected, the CW-IMP trace shows significant deviations and an offset up to 0.7 dB. For gain setting 30, it can be seen that a maximum DR of 25 dB is achieved at an error of CW-IMP smaller than 1.5 dB, equivalent to the defined target. The gain has not been further increased, as the sensitivity is already sufficient for the proposed TEM cell. To conclude, the *B200mini* offers enough DR to perform PD measurements with a preselector covering the entire frequency range of *CISPR* band C/D. If QPD measurements want to be tackled, the preselector bandwidth has to be drastically reduced.

III. Front-End Extension

The front-end extension announced in Section I works as an upconversion stage. The centerpiece of the development is a highly linear mixer, which provides sufficient DR to perform compliant QPD measurements in *CISPR* band C/D [14]. It was shown that the NF is comparable to professional receivers with a maximum of 14 dB. To overcome the problem with downconversion spurs of homodyne receivers, the output of the front end is bandpass-filtered suppressing frequency content at LO harmonics of the SDR. Mostly off-the-shelf components on an *FR-4* substrate are used, enabling a simple manufacturing process at low costs.

Owing to an overlap of the RF and IF frequency bands, the initial design had problems with an insufficient suppression failing the 40-dBc requirement for CW signals. Furthermore, the matching needed to be improved in band D, because of a design error in the printed circuit board (PCB) layer stack up.

In the following, a redesigned upconversion stage, improving the discussed problems, is characterized. While a detailed block diagram and a picture of the realization are given in Fig. 11, the used key components are listed in Table I.

A. Frequency Planning

The front end has two preselector paths for *CISPR* bands C and D, respectively. The first path is for frequencies below 300 MHz and converts the upper side band to the IF located at 1.227 GHz. Above 300 MHz, the second path is utilized, mixing up the lower side band. In Fig. 12, the insertion loss (IL) and VSWR are visualized. The VSWR exceeds the required value of 2:1 with a maximum of 2.28:1 at 380 MHz. As the utilized mixer is sensitive to load mismatches introduced by the IF filter BP2, this behavior could not be avoided unless the low-noise amplifier

TABLE I
Key Component List of the Upconversion Stage

Name	Part	Manufacturer
LP1	*RLP-320+*	Mini-Circuits
HP1	*RHP-260+*	Mini-Circuits
BP1	*BPF-510C+*	Mini-Circuits
MX	*SYM-30DHW+*	Mini-Circuits
BP2/4	*TA1227BB*	Tai-Saw
LNA	*TQP3M9009*	Qorvo
BP3	*TA1228BB*	Tai-Saw
AT1/2	*F1950*	Renesas
LP2	*LFCN-1000+*	Mini-Circuits
HP2	*HFCN-1500+*	Mini-Circuits
PLL	*ADF4002*	Analog Devices
Synthesizer	*LTC6948-2*	Linear Technologies

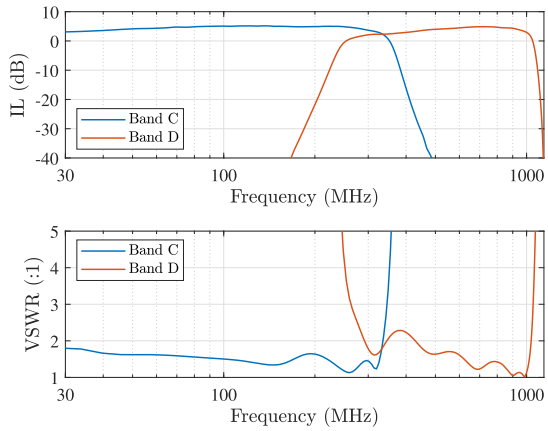

Fig. 12. Transfer characteristics of the upconversion stage measured at RF IN and RF OUT.

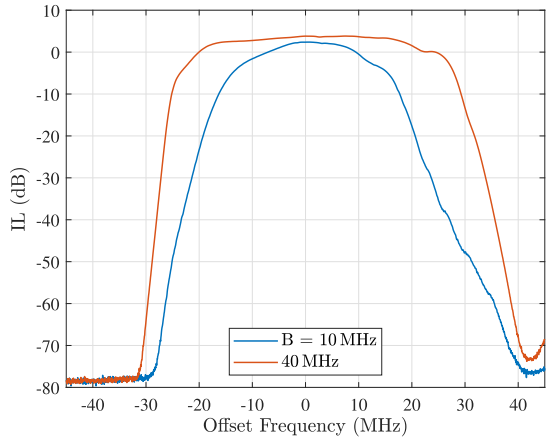

Fig. 13. IF response of the available filters implemented in the upconversion stage measured at $f_0 = f_{LO} - f_{IF} = 500$ MHz.

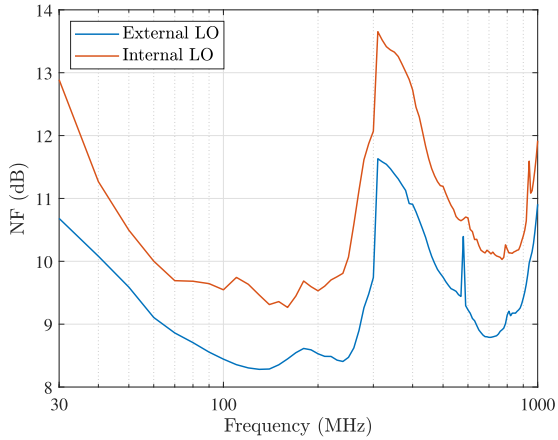

Fig. 14. Performance comparison of the NF for different LO configurations.

(LNA) changes position with BP2 providing a broadband match to the mixer. The downside of this approach is that LNAs usually cannot provide sufficient linearity to handle the output power of such mixers degrading the overall DR, which is crucial for the dedicated application. Hence, it is to choose applying a forced match for measurements in the failing frequency range by use of, e.g., an attenuator or an LNA. Intentionally, no amplification has been implemented at the RF input as the additional gain would decrease the compression level of the mixer and, thus, is not recommended by *CISPR 16-1-1*. As suggested in Section II-E, inserting additional attenuation is the way to go if the required sensitivity allows to which is treated hereinafter in Section III-B.

Two different IF bandwidths are available with a usable bandwidth of 10 and 40 MHz (see Fig. 13). As the preselection filter BP1 offers an IL of more than 50 dB in the IF frequency range, the RF–IF leakage suppression is a minor issue now. In addition, the image frequency suppression of the *B200mini* has been verified to be compliant and in conjunction with the front-end extension; this requirement is fulfilled as well for the specified IF bandwidths. The two different IF paths have an impulse bandwidth of 20 and 62 MHz. It was shown in Fig. 9 that with the reduction of the preselector bandwidth to the latter value, QPD measurements might become possible for the SDR.

B. Sensitivity

The sensitivity of the upconversion stage is mainly dominated by the mixer in front of the LNA. Besides conversion loss, the feedthrough of phase noise from the LO into the IF band plays an important role for the NF. Even with sufficient frequency distance between the LO carrier and the IF passband, wideband noise from the voltage-controlled oscillator (VCO) might decrease the mixer performance. As highly linear mixers require a large LO power level, i.e., 20 dBm, enough LO-IF isolation has to be provided to suppress VCO noise below thermal noise power density. To further lower the discussed feedthrough, low- and high-pass filters (LP2 and HP2) are added in front of the implemented frequency synthesizer. With the step attenuator, the carrier power is leveled to the desired 20 dBm.

Traditionally, LO synthesizers are realized with a PLL generating integer or fractional multiples of the provided reference frequency. The phase frequency detector (PFD) determines the switching frequency of the charge pump (CP) tuning the VCO. Periodically repeating CP spurs offset from the LO carrier occur and might cause interference due to feedthrough into the IF path. Therefore, a dual-loop PLL was implemented to shift the main synthesizer's CP spurs out of the IF frequency range. The first PLL is utilized for mainly two purposes: First, the loop bandwidth is rather low to clean a potentially noisy reference clock; second, integer multiples of the divided reference can be generated between 100 and 200 MHz, feeding the main PLL. With the synthesizer, integer/fractional multiples of the input frequency are generated, free of CP spurs at the IF frequency range and of sufficient tuning accuracy.

To proof the implemented concept, the NF of the upconversion stage is compared using an external bandpass filtered LO (see Fig. 14). In the redesign, the maximum NF could be kept below 14 dB as for the initial version. The internal LO decreases the sensitivity by approximately 2 dB compared to the externally applied source. Although the measurement setup was shielded, leakage due to interference from *LTE* and *DVB-T* base stations in the close vicinity coupled into peripheral cables connected with the setup. The noise power requirement P_{min} from Section II-D has its minimum at 1 GHz of -80 dBm. Thus, an NF requirement can be derived taking the maximum noise amplification of $G_N^{PD} = 10$ dB and $SNR_{min} = 6$ dB through $NF = P_{min} - SNR_{min} - G_N^{PD} + 174\,\text{dBm/Hz} - 10\log_{10} B_N^{CISPR} = 29$ dB into account. As the achieved NF is 15 dB better than the calculated value, forced matching the upconversion stage is the best choice to achieve a compliant measurement setup with the proposed TEM cell.

C. Available DR

While the upconversion stage fulfills the CW requirements, it is to be shown how much DR measuring *CISPR* pulses is available. To do so, the stage was tuned to two different frequencies located in bands C and D, namely, $f_0 = f_{LO} \pm f_{IF} = 60$ and 500 MHz. The compression from linear gain is measured with a

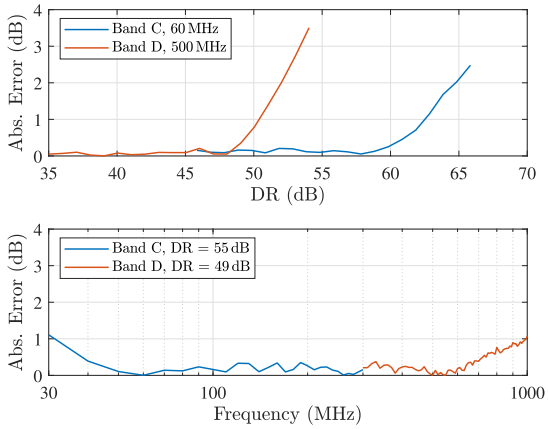

Fig. 15. Broadband DR of the upconversion stage measuring compression from linear gain and the error over frequency for a certain power level setting.

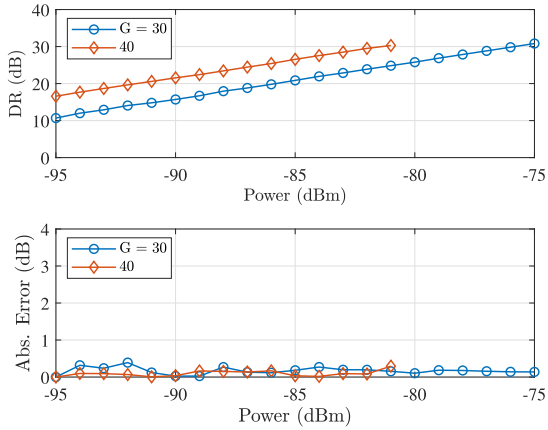

Fig. 16. Achieved DR over input power and the corresponding compression from linear gain for impulses.

fully compliant EMI receiver at the output RF OUT.[3] Comparing the measured peak output power of the *CISPR* filter with the maximum sensitivity level due to the NF yields the error versus the DR (see Fig. 15). To verify the performance over band C/D, the error was calculated by comparing the impulse power with a calibrated CW signal indicating the same level if no saturation occurs. Although the measurements show that a DR of more than 60 dB is available at the certain frequency spot, the broadband performance degrades for lower frequencies and forced to reduce the power level to a DR of 55 dB. To conclude, a DR of 55 and 49 dB is achieved in bands C and D, respectively, with a maximum error of 1 dB. Even though bands C and D are separate frequency ranges, *CISPR 16-1-1* unites them by specifying the same requirements, e.g., the OVF. Strangely, in fact, the actual version of the norm has reduced the weighting range of the QPD to a DR of 26 dB in band D. As the redesigned upconversion stage has two preselector paths covering band C/D separately, it is assumed that an OVF of 26 dB is sufficient between 300 MHz and 1 GHz. Hence, the upconversion stage provides enough DR to perform compliant QPD measurements.

IV. Performance Improvement

The performance analysis of the *B200mini* in Section II showed that the DR is limited to 25 dB for broadband impulses. Although this is sufficient for compliant PD measurements, the SDR alone fails the 40-dBc requirement for CW signals due to downconversion spurs. With the presented upconversion stage from Section III, the mentioned problem is solved as the bandpass filtered output suppresses frequency content apart from the fundamental downconversion product. Moreover, the implemented IF filters decrease the impulse bandwidth at the SDR input, and thus, the available DR is increased for broadband impulses. In this section, the achievable DR for impulses of the *B200mini* in conjunction with the redesigned upconversion stage is investigated.

[3]EMI Receiver: Keysight Technologies *MXE N9038A*.

A. Performance at Full ABW

First of all, the performance at full ABW of the SDR is examined utilizing the 40-MHz path of the upconversion stage. In principal, the configuration of the SDR has been adopted from Section II-C with the only difference that the *B200mini* was tuned to $f_0 = 1.227$ GHz with the IF located at $f_{\mathrm{IF}} = -500$ kHz. The IF was shifted to a lower frequency to avoid suppressing the signal for a lower AAF bandwidth, which is covered subsequently. In Fig. 16, the DR over input power and the deviation from linear gain is depicted for two different gain settings. The upconversion stage was tuned to 60 MHz, and the impulse power was increased until full-scale resolution of the ADC was reached. Obviously, the full DR of the ADC is accessible as the error stays negligible over the entire power sweep. The maximum DR is achieved for both the gain settings at 31 dB matching the analytically derived values from Fig. 9 very well. The quantization noise power level was low enough to resolve the noise floor of the upconversion stage, maintaining the NF in the range from Fig. 14. To increase the ABW of the *B200mini*, it is possible to overclock the RFIC *AD9364* up to 128 MSa/s and bypass the AAF filter, which limits the ABW to 20 MHz. Currently, this feature is not supported by the *UHD* driver from Ettus Research interfacing the *B200mini* and is, thus, future work to be verified. Although the IF filters of the upconversion stage provide sufficient selectivity of aliases, it is questionable if the spurious performance satisfies *CISPR* standards when the AAF section is bypassed.

B. Impact of AAF Bandwidth

As the available DR at full ABW is still insufficient to perform compliant QPD measurements, further bandwidth reduction of the AAF is necessary. The minimum bandwidth to properly resolve the *CISPR* filter is 1 MHz. Hence, to investigate the maximum achievable DR of the SDR, the AAF cutoff frequency is tuned to this value. Next, a power sweep of the impulses is performed for different gain settings. In Fig. 17, the deviation from linear gain is depicted. Obviously, using the 40-MHz path of the upconversion stage allows a DR up to 43 and 47 dB for

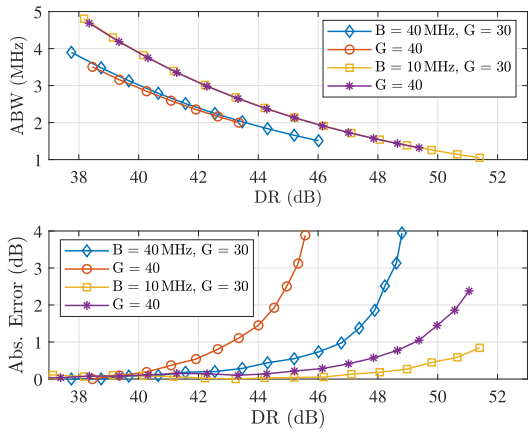

Fig. 17. Absolute error of the deviation from linear gain and the available ABW over achieved DR for impulses.

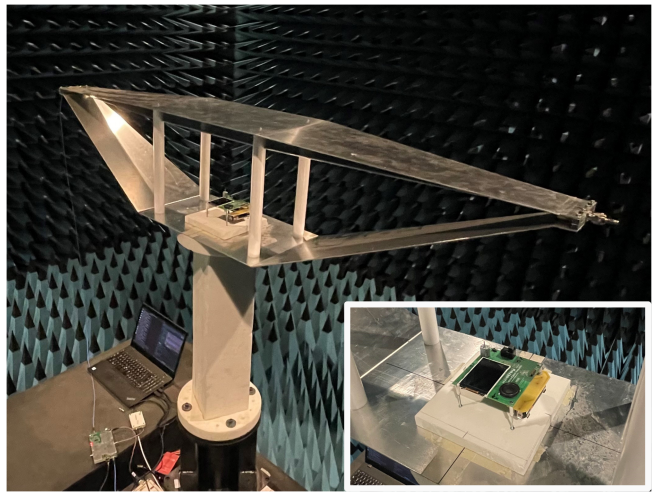

Fig. 18. TEM-cell-based setup placed in an anechoic chamber. The reference EUT is magnified in the lower right.

gains 40 and 30, respectively. With the 10-MHz path, the linearity requirements of the SDR can be further reduced, achieving the target DR of 51 dB defined for the QPD. Based on the backoff level from full-scale resolution of the ADC, the maximum ABW at the achieved DR can be calculated. While in *CISPR* band C, the ABW is limited to 1 MHz, in band D, a DR of 38 dB is sufficient, which allows increasing the ABW to 5 MHz. While PD measurements can be performed at full bandwidth, the QPD forces to strongly reduce bandwidths coming along with an increased frequency scan time.

C. Remarks

Further verification measurements on the transmitter path incorporated in the *B200mini* have been made. The idea was to embed the SDR's output as external LO section in the upconversion stage aiming to further reduce the costs. The *B200mini* achieves an output power between 10 and 14 dBm in the mentioned LO tuning range. With an external gain block, it is possible to generate the desired 20 dBm driving the highly linear mixer. Besides the explained problem with CP spurs (see Section III-B), strong coupling effects of LO harmonics between the transmit and receive path forced to drop this idea.

V. Verification Against Accredited Test Sites

To verify the discussed setup comprising the TEM cell from [6], the improved front-end extension, and the SDR *B200mini*, the emission spectra of an EUT according to *CISPR 32* are measured. The battery-powered test device incorporates several radiation sources, e.g., dc–dc converters, an LCD display, a dc motor, and a class-D audio amplifier on a PCB with a size of 10 cm by 10 cm. The results from three different accredited EMC test houses using, i.e., a 3-m SAC, a 5-m SAC, and a 3-m fully anechoic chamber (FAC), are taken as reference for comparisons with our low-cost system. In addition, measurements with a professional GTEM cell have been made to identify uncertainties caused by limitations of the correlation algorithm from Section II-D.[4] It must be mentioned that the repeatability and accuracy of different test sites have been investigated by a round robin test in [26], [27], and [28]. Owing to setup-related deviations, an uncertainty of up to ± 10 dB has been experienced, which may also be expected for the presented results.

A. Measurement Scenario

To prevent from interference coupling into the open TEM cell, the measurements have been made in a shielded anechoic chamber (see Fig. 18). It is recommended by *MIL-STD 462F RS105* to separate open TEM cells from reflecting surfaces at least two times the septum height, i.e., ≥ 600 mm, which was achieved by a Rohacell foam support [22].

The configuration of the SDR and the front end has been adopted from Section IV-A. Furthermore, the signal analysis was made according to Section II-D using the PD over a recording length of 1 s. The absolute power level calibration of the receiver in conjunction with applied cables was made with a calibrated CW source.

In [6], the test volume of the TEM cell was verified with a field probe covering the EUT's dimensions. With the second port of the cell, it is possible to crosscheck field homogeneity deviations in loaded conditions. It is assumed that the total losses of the cell are mainly caused by energy coupling into higher order modes, which can cause resonances of the electric field in the cavity. To be compliant, the losses of the empty cell have to be smaller than 1 dB, which are calculated with the S-parameters of the cell according to

$$|10\log_{10}(S_{11}^2 + S_{21}^2)| \leq 1 \text{ dB}. \tag{11}$$

The maximum losses of (11) are depicted in Fig. 19 for the unloaded cell and in loaded conditions. Obviously, the loaded cell slightly exceeds the bound for frequencies above 700 MHz due

[4]The *Teseq 500* was used in conjunction with the EMI receiver *MXE N9028A* from Keysight Technologies fully complying to *CISPR 16-1-1* and *CISPR 32*.

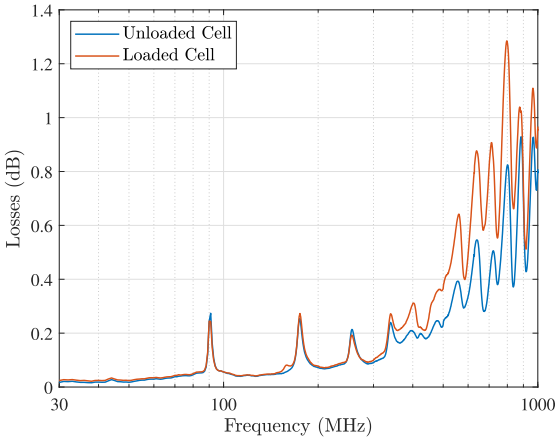

Fig. 19. Total losses of the TEM cell from [6] unloaded and loaded with the EUT.

to higher order mode excitation. It is to be noted that resonances in the test volume potentially lead to measurement deviations, which have to be taken into account when interpreting emission spectra at critical frequencies.

B. Results

The analytic correlation algorithm for TEM cells is a worst case model as it superposes absolute power values of three EUT positions [see (6)], aiming to preserve the maximum emission spectrum. In Fig. 20, the comparison of the emission spectra from different test sites with the proposed low-cost setup is depicted. As an overlay of noisy spectra impedes the visibility of differences in field strength, the maximum peaks with a minimum separation of 1 MHz have been depicted to highlight the results. It was verified in advance that the output power of the TEM cell is not saturating the SDR-based receiver. It can be directly seen from all the subfigures that the TEM cell yields a higher field strength than the GTEM based setup, although the shape of the spectrum is almost the same up to 700 MHz. According to [28], potential measurement uncertainty sources causing this offset are, e.g., the repeatability of the EUT, field homogeneity perturbations of the loaded cell, and thermal drifting of the setup. Above 700 MHz, resonances in the TEM cell cause an over estimation of the spectrum, which was predicted in Fig. 19.

The SACs show a relatively high spectrum amplitude compared to the FAC for frequencies between 30 and 50 MHz. In this range, maximum field strengths occurred for the vertical polarization of the receiving antenna at a height of only 1 m above the ground plane. Operating large EMI antennas that close to a reflecting surface influences their transfer characteristics and causes in this case a higher field strength. As the antenna height is kept constant at approximately 2 m in the FAC, the measurements show a better correlation with the TEM-based results.

Besides test site, EUT, and correlation algorithm-related deviations, the envelopes of the emitted spectra show a good agreement with the low-cost setup considering typical tolerances

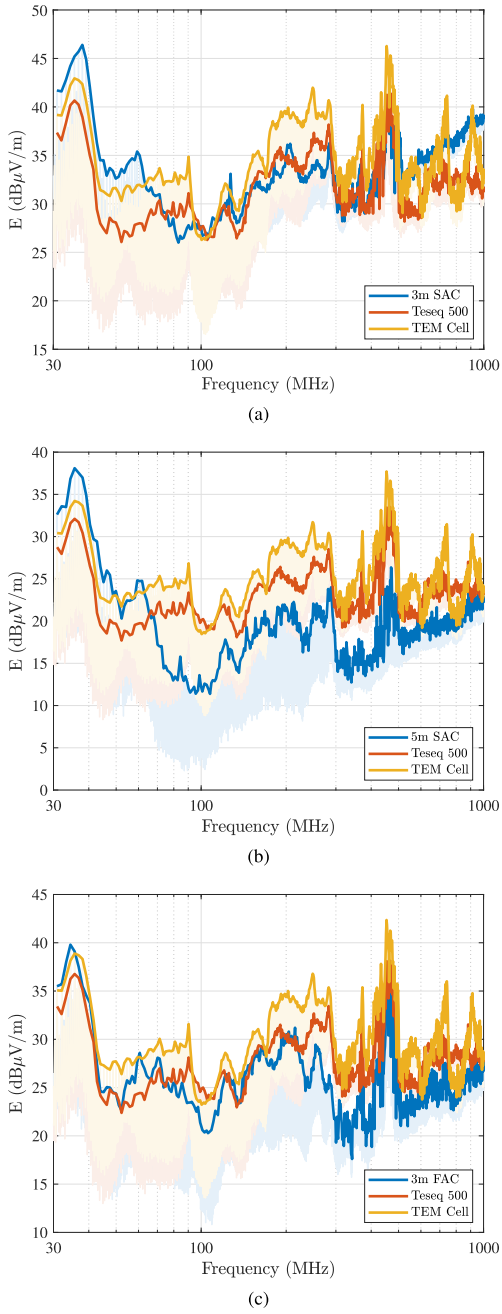

Fig. 20. Comparison of the radiated emission spectra from the (a) 3-m SAC, (b) 5-m SAC, and (c) 3-m FAC with the measurements made using a *Teseq 500* GTEM cell and the proposed low-cost setup. The results for the 5-m SAC have been recalculated by the EMC test house to an equivalent distance of 10 m. The maximum field strength of the traces is emphasized by the visualization of the spectrum peaks separated by at least 1 MHz.

analyzed in the mentioned round robin tests. Hence, the feasibility of performing radiated emission testing has been further verified, carrying out a realistic test case, supplementary to *CISPR 16-1-1* procedures.

VI. Conclusion

Throughout this article, the suitability of the low-cost SDR *B200mini* from Ettus Research was investigated in terms of

radiated emission measurements in *CISPR* band C/D. Based on a measurement setup typical for precompliance purposes, i.e., a TEM cell, the performance was analyzed. Besides sufficient frequency accuracy, matching, and sensitivity, it was shown that the DR of the *B200mini* is high enough to perform PD measurements at an ABW of 20 MHz. The main problem, the homodyne-based SDR was suffering from, is downconversion spurs making compliant measurements impossible without suppressing frequency content at LO harmonics. It was discussed that this problem can be solved by applying additional preselection filters with the downside that the number of required filters increases as the investigated frequency decreases. In addition, the SDR's analog front end did not provide sufficient linearity for QPD measurements, representing the benchmark for EMI receivers, without reducing the preselector bandwidth drastically. To solve the mentioned problems, a highly linear upconversion stage was utilized, which was verified to satisfy QPD requirements. The bandpass-filtered output reduced the impulse bandwidth at the SDR input to the analytically derived target value and suppressed frequency content apart from the fundamental downconversion product. The measurement results of the *B200mini* in conjunction with the upconversion stage indicated that QPD measurements are possible. To achieve the required DR, it was necessary to reduce the bandwidth of the AAF in front of the ADC to 1 MHz in band C and to 5 MHz in band D. As a final step, the whole measurement setup comprising a TEM cell, the front-end extension, and the *B200mini* was verified by characterizing an EUT. The measurement results of the low-cost setup showed a comparable performance with fully compliant systems. To conclude, the most challenging requirements specified in *CISPR 16-1-1* were tackled successfully using a low-cost radiated emission measurement setup based on a homodyne SDR. By carrying out a realistic test case, the reliable estimation of emission spectra in advance was demonstrated.

Appendix A
Antenna Height Scan of the Mirrored Dipole

To fully understand the correlation algorithm used in Section II-D, the antenna height scan in an SAC is explained. According to Fig. 21, the EUT is placed on a table $h_\mathrm{T} = 0.8\ \mathrm{m}$ above an ideal and infinitely extended ground plane. The receiving antenna is positioned $s = 10\ \mathrm{m}$ apart and is variable in height from $h_\mathrm{A} = 1$ to 4 m. The radiation pattern of the EUT is modeled as a dipole. Analytically, the ground plane is treated by mirroring the radiation source. Usually, two worst case scenarios are assumed for the correlation algorithm. For vertical and horizontal polarizations of the receiving antenna, maximum field strengths of the EUT occur when it is polarized in the same direction. The electric field of a dipole varies with the elevation angle θ according to $\sin\theta e^{-jk_0 r}/r$. After superposing the mirrored dipoles, the geometrical factor g_max is given in (12) for horizontal and vertical polarizations. By taking the maximum of both equations over frequency and antenna height, the maximum field strength in far-field conditions is derived. It is possible to adjust the SAC scenario, e.g., to an FAC, by simply neglecting the secondary terms in (12), as no ground plane is used in this test site

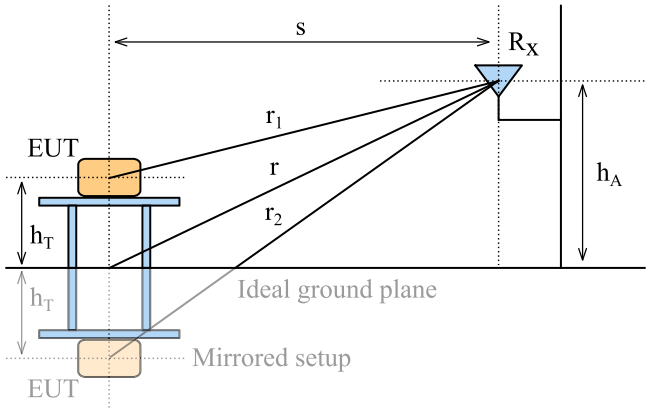

Fig. 21. Scenario of the mirrored EUT problem in an SAC with the reflecting ground plane.

$$g_\mathrm{max} = \begin{cases} \left| \frac{e^{-jk_0 r_1}}{r_1} - \frac{e^{-jk_0 r_2}}{r_2} \right|_\mathrm{max} & \text{hor. pol.} \\ \left| \frac{s^2}{r_1^2}\frac{e^{-jk_0 r_1}}{r_1} + \frac{s^2}{r_2^2}\frac{e^{-jk_0 r_2}}{r_2} \right|_\mathrm{max} & \text{vert. pol.} \end{cases}. \quad (12)$$

Appendix B
Signal Path Model of the SDR

The signal model of the SDR used in Section II-F to estimate the performance for transient signals implies several simplifications, which are discussed in the following. According to the receiver topology of the *B200mini*, the analytic equation (1) of a homodyne receiver is extended by

$$x_\mathrm{IF}(t) = [G(x_\mathrm{RF}(t) * h_\mathrm{PRE}(t))e^{-jw_\mathrm{LO}t}] * h_\mathrm{AAF}(t) * h_\mathrm{CISPR}(t). \quad (13)$$

The respective impulse responses of the preselector, the AAF, and the *CISPR* filter are denoted by $h(t)$. To derive the required gain G of the system for full-scale resolution of the ADC, the known peak output of the preselector and the AAF are brought into relation. Therefore, the input stimulus is chosen to be an impulse according to $x_\mathrm{RF}(t) = v\tau\delta(t)$

$$\frac{\hat{V}_\mathrm{AAF}}{\hat{V}_\mathrm{PRE}} = \frac{G\max\{|(h_\mathrm{PRE}(t)e^{-jw_\mathrm{LO}t}) * h_\mathrm{AAF}(t)|\}}{\max\{|(h_\mathrm{PRE}(t)|\}}. \quad (14)$$

Simplifying (14), it is assumed that the frequency shifted transfer characteristic of the preselector $h_\mathrm{PRE}(t)\cdot e^{-jw_\mathrm{LO}t}$ has no impact on the impulse response of the AAF $h_\mathrm{AAF}(t)$. The peak output of a filter can be defined by $\hat{V} = \max\{|v\tau\delta(t) * h(t)|\} = v\tau B_I$ and allows us to derive the gain by

$$G = \frac{\hat{V}_\mathrm{AAF}}{\hat{V}_\mathrm{PRE}}\frac{B_I^{PRE}}{B_I^{AAF}}. \quad (15)$$

In further calculations of this work, the influence of preceding filter characteristics is neglected. In addition, I/Q imbalances are not considered as their effect is assumed to be negligible for RF-link budget calculations.

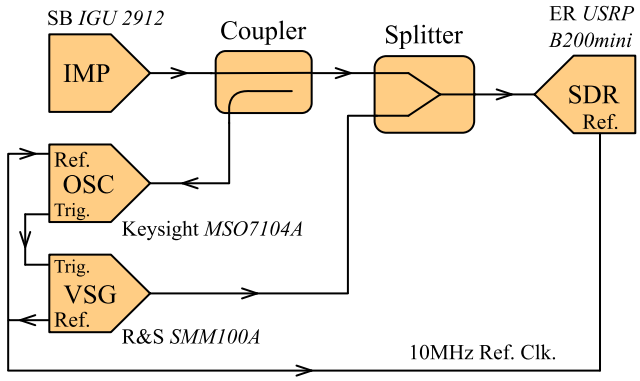

Fig. 22. Setup for coherent averaging of *CISPR* impulses.

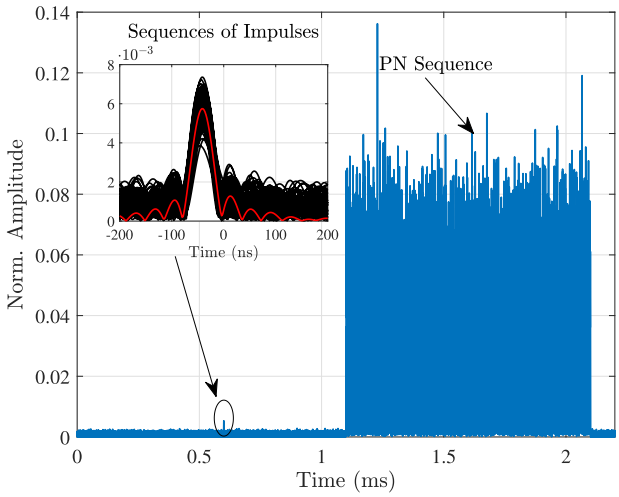

Fig. 23. Visualization of the averaging process.

With the derived gain, it is now possible to calculate the downconverted thermal noise level. The PSD of the random signal $n(t)$ can be derived using the autocorrelation function $\tilde{r}(\tau)$:

$$\begin{aligned}\tilde{r}(\tau) &= E\{[n(t)e^{-jw_{\mathrm{LO}}t}][n(t-\tau)e^{-jw_{\mathrm{LO}}(t-\tau)}]^*\} \\ &= Gr(\tau)e^{-jw_{\mathrm{LO}}\tau}. \end{aligned} \tag{16}$$

The desired PSD is evaluated by taking the Fourier transform of $\tilde{r}(\tau)$

$$\tilde{R}(jw) = \mathcal{F}\{Gr(\tau)e^{-jw_{\mathrm{LO}}\tau}\} = \frac{kT_0}{2}. \tag{17}$$

By introducing the noise bandwidth $\mathrm{B_N} = \int |H(jw)|^2 dw$, the noise power level for a certain filter further simplifies to

$$P_{\mathrm{N}} = \frac{kT_0}{2}\int_{-\infty}^{\infty} |H(jw)|^2 dw = \frac{kT_0}{2} B_{\mathrm{N}}. \tag{18}$$

To summarize, the most important signal definitions, used in this article, regarding impulses and thermal noise have been explained.

Appendix C
Time Coherent Averaging of *CISPR* Pulses

To test EMI receivers according to *CISPR 16-1-1*, an impulse source generating extremely broadband transients of high amplitude is necessary. In the investigated frequency range of *CISPR* band C/D reaching from 30 MHz to 1 GHz, such generators have to achieve an almost rectangular output over 300 ps and an amplitude of 73.3 V into a 50-Ω load. The source used in this article, i.e., Schwarzbeck *IGU 2912*, has reed contacts implemented to achieve the highly demanding requirements. Owing to jittering of the mechanical switch contacts, synchronization of the impulse source with other measurement equipment is difficult. As, in this article, a low-cost receiver with potentially limited DR for such broadband signals is investigated, it was of high interest to average the impulses in time domain for lowering measurement uncertainties through thermal noise. To synchronize time bases between the SDR and the impulse source, an external trigger system was used (see Fig. 22). An oscilloscope (OSC) monitors the output of the impulse generator (IMP) and outputs a trigger to a vector-signal generator (VSG), which transmits a pseudonoise (PN) sequence following the impulse to the SDR, as depicted in Fig. 23. Under ideal conditions, the delay between the received correlation sequence and the impulse is constant. Thus, it is possible to detect the events coherently by correlating the measurements with the original PN sequence. The phase information for equalizing the aligned traces is taken at the decision point with maximum SNR of the first impulse event. After averaging the baseband data sampled by the SDR, the signal can be further processed by the *CISPR* filter.

The setup suffers from imperfect synchronization of the SDR with the 10-MHz reference clock. As the *B200mini* incorporates a TCXO, which is trimmed digitally, the measured delay between the impulse and the PN sequence is jittering. This problem is further intensified by the VSG. Although the propagation delay of the oscilloscope's trigger unit is almost constant, the VSG, i.e., R&S *SMM100A*, cannot be triggered infinitely fast. As the arbitrary waveform generator is running at 500 MSa/s, the timing response is limited to this sampling rate. In total, a maximum jitter of 20 ns was achieved with this setup. Owing to the relatively long impulse response of the *CISPR* filter described by (3), the jitter has a negligible impact on the amplitude accuracy of the measured impulses.

References

[1] I. Grobler and M. Gitau, "Low cost power lead extended pre-compliance conducted EMI measurement setup and diagnostics with compact LISN," in *Proc. IEEE ECCE Asia Downunder*, Melbourne, VIC, Australia, 2013, pp. 1144–1149, doi: 10.1109/ECCE-Asia.2013.6579252.

[2] J. Pontt et al., "Developing a simple, modern and cost effective system for EMC pre-compliance measurements of conducted emissions," in *Proc. IEEE Eur. Conf. Power Electron. Appl.*, Aalborg, Denmark, 2007, pp. 1–7, doi: 10.1109/EPE.2007.4417737.

[3] D. Sakulhirirak, V. Tarateeraseth, W. Khan-Ngern, and N. Yoothanom, "Design of high performance and low cost line impedance stabilization network for university power electronics and EMC laboratories," in *Proc. IEEE 7th Int. Conf. Power Electron. Drive Syst.*, Bangkok, Thailand, 2007, pp. 284–289, doi: 10.1109/PEDS.2007.4487715.

[4] J. Yousaf, W. Nah, M. I. Hussein, J. G. Yang, A. Altaf, and M. Elahi, "Characterization of reverberation chamber—A comprehensive review," *IEEE Access*, vol. 8, pp. 226591–226608, 2020, doi: 10.1109/ACCESS.2020.3045028.

[5] A. Takach, F. Ndagijimana, J. Jomaah, and M. Al-Husseini, "3D-printed low-cost and lightweight TEM Cell," in *Proc. IEEE Int. Conf. High Perform. Comput. Simul.*, 2018, pp. 47–50.
[6] C. Spindelberger, G. Giannetti, and H. Arthaber, "Increasing the test-volume of open TEM cells by using an asymmetric design," in *Proc. IEEE Kleinheubach Conf.*, Miltenberg, Germany, 2022, pp. 1–4.
[7] *Specification for Radio Disturbance and Immunity Measuring Apparatus and Methods—Part 1: Radio Disturbance and Immunity Measuring Apparatus—Measuring Apparatus*, CISPR 16-1-1, 2019.
[8] M. F. A. Rahim, "Evolution and trends of EMI receiver," in *Proc. IEEE Int. RF Microw. Conf.*, Penang, Malaysia, 2013, pp. 362–367, doi: 10.1109/RFM.2013.6757285.
[9] S. Braun, T. Donauer, and P. Russer, "A real-time time-domain EMI measurement system for full-compliance measurements according to CISPR 16-1-1," *IEEE Trans. Electromagn. Compat.*, vol. 50, no. 2, pp. 259–267, May 2008, doi: 10.1109/TEMC.2008.918980.
[10] M. Parvis, G. Perrone, and A. Vallan, "A precompliance EMC test-set based on a sampling oscilloscope," in *Proc. IEEE 19th Instrum. Meas. Technol. Conf.*, Anchorage, AK, USA, 2002, pp. 1197–1201, doi: 10.1109/IMTC.2002.1007128.
[11] C. De Capua and C. Landi, "A digital measurement station for RF-conducted emissions monitoring," *IEEE Trans. Instrum. Meas.*, vol. 51, no. 6, pp. 1363–1366, Dec. 2002, doi: 10.1109/TIM.2002.808029.
[12] A. A. Abidi, "The path to the software-defined radio receiver," *IEEE J. Solid-State Circuits*, vol. 42, no. 5, pp. 954–966, May 2007, doi: 10.1109/JSSC.2007.894307.
[13] C. Spindelberger and H. Arthaber, "Out-of-the-box performance of popular SDRs for EMC pre-compliance measurements," in *Proc. Int. Symp. Electromagn. Compat.*, Gothenburg, Sweden, 2022, pp. 677–682, doi: 10.1109/EMCEurope51680.2022.9901003.
[14] C. Spindelberger and H. Arthaber, "Improving the performance of direct-conversion SDRs for radiated precompliance measurements," *IEEE Lett. Electromagn. Compat. Pract. Appl.*, vol. 5, no. 1, pp. 22–26, Mar. 2023, doi: 10.1109/LEMCPA.2022.3227409.
[15] *Electromagnetic Compatibility of Multimedia Equipment—Emission Requirements*, CISPR 32, 2015.
[16] D. B. Geselowitz, "Response of ideal radio noise meter to continuous sine wave, recurrent impulses, and random noise," *IRE Trans. Radio Freq. Interference*, vol. RFI-3, no. 1, pp. 2–11, May 1961, doi: 10.1109/RFI.1961.6541594.
[17] R. L. Belding, "Receiver measurements near the noise floor," in *Proc. IEEE Int. Symp. Electromagn. Compat.*, San Diego, CA, USA, 1986, pp. 1–8, doi: 10.1109/ISEMC.1986.7568204.
[18] F. Krug, S. Braun, Y. Kishida, and P. Russer, "A novel digital quasi-peak detector for time-domain measurements," in *Proc. IEEE 33rd Eur. Microw. Conf.*, Munich, Germany, 2003, pp. 1027–1030, doi: 10.1109/EUMA.2003.340834.
[19] *RF Agile Transceiver AD9364, Data Sheet*, Analog Devices, Norwood, MA, USA. Accessed: Jun. 2023. [Online]. Available: https://www.analog.com/media/en/technical-documentation/data-sheets/ad9364.pdf
[20] E. Klumperink and A. Molnar, "Interference robust, flexible radio receivers in CMOS," *IEEE RFIC Virtual J.*, vol. 6, no. 6, Oct. 2014, doi: 10.1109/RFICVJ.2017.0000006.
[21] P. Wilson, "On correlating TEM cell and OATS emission measurements," *IEEE Trans. Electromagn. Compat.*, vol. 37, no. 1, pp. 1–16, Feb. 1995, doi: 10.1109/15.350235.
[22] *Electromagnetic Compatibility (EMC)—Part 4-20: Testing and Measurement Techniques—Emission and Immunity Testing in Transverse Electromagnetic (TEM) Waveguides*, Standard IEC 61000-4-20:2010, 2010.
[23] S. Braun, A. Frech, and P. Russer, "CISPR specification and measurement uncertainty of the time-domain EMI measurement system," in *Proc. IEEE Int. Symp. Electromagn. Compat.*, Detroit, MI, USA, 2008, pp. 1–4, doi: 10.1109/ISEMC.2008.4652078.
[24] *AD9364 Reference Manual UG-673*, Analog Devices, Norwood, MA, USA. Accessed: Jun. 2023. [Online]. Available: https://www.analog.com/media/cn/technical-documentation/user-guides/ad9364_reference_manual_ug-673.pdf
[25] *RF Performance Measurements B200mini*. Accessed: Jun. 2023. [Online]. Available: https://kb.ettus.com/images/a/ae/B200mini_B205_RF_Performance_Data_20160119.pdf
[26] J. J. Goedbloed and P. A. Beeckman, "Uncertainty analysis of the CISPR/a radiated emission round-robin test results," *IEEE Trans. Electromagn. Compat.*, vol. 46, no. 2, pp. 246–262, May 2004, doi: 10.1109/TEMC.2004.826892.
[27] P. A. Beeckman and J. J. Goedbloed, "Results of the CISPR/A radiated emission round robin test," in *Proc. IEEE/EMC Int. Symp. Electromagn. Compat.*, Montreal, QC, Canada, 2001, pp. 475–480, doi: 10.1109/ISEMC.2001.950687.
[28] A. Nothofer, D. Bozec, A. Marvin, M. Alexander, and L. McCormack, "The use of GTEM cells for EMC measurements—Measurement Good Practice Guide no 65," National Physical Laboratory, Teddington, U.K., and York EMC Services Ltd., Heslington, U.K. Accessed: Jun. 2023. [Online]. Available: https://emcfastpass.com/wp-content/uploads/2020/02/GTEM_measurement_guide.pdf

Christian Spindelberger (Student Member, IEEE) received the Dipl.-Ing. degree in telecommunications in 2019 from the Vienna University of Technology, Vienna, Austria, where he is currently working toward the Dr.Techn. degree in low-cost receivers for EMC purposes.

In 2018, he joined the Microwave Engineering Group, Institute of Electrodynamics, Microwave, and Circuit Engineering, Vienna University of Technology. Based on his gained knowledge in his research area, he has organized and held a seminar on precompliance measurements. His current research interests include software-defined radios, electromagnetic compatibility (EMC) measurements, EMC norms, and transverse electromagnetic cells.

Holger Arthaber (Senior Member, IEEE) received the Dr.Techn. and Habilitation degrees in RF and information technology from the Vienna University of Technology, Vienna, Austria, in 2004 and 2017, respectively.

He is currently an Associate Professor and the Head of the Microwave Engineering Group, Institute of Electrodynamics, Microwave and Circuit Engineering, Vienna University of Technology. He has (co)authored more than 120 peer-reviewed publications. His research interests include microwave material characterization, indoor localization, antenna design and measurement, electromagnetic compatibility measurements, software-defined radios, and RF system design.

Dr. Arthaber is a core Technical Program Committee Member of International Workshop on Integrated Nonlinear Microwave and Millimetre-wave Circuits and an Editorial Board Member of *International Journal of RF and Microwave Computer-Aided Engineering*. He was a Guest Editor for various IEEE and MPDI journals.